

# Enhancement of R123 Pool Boiling by the Addition of N-Hexane

---

Mark A. Kedzierski

March 1996



**U.S. Department of Commerce**  
Ronald H. Brown, *Secretary*  
Technology Administration  
Mary L. Good, *Under Secretary for Technology*  
National Institute of Standards and Technology  
Arati Prabhakar, *Director*

*Prepared for:*  
**U.S. Department of Energy**  
Office of Building Technology  
1000 Independence Avenue  
Washington, DC 20585



## ABSTRACT

This paper presents the heat transfer data used to file international patent WO 94/18282. The data consisted of pool boiling performance of a GEWA-T<sup>TM</sup> surface for three fluids: (1) pure R123, (2) R123/n-hexane (99/1), and (3) R123/n-hexane (98/2). The heat flux and the wall superheat were measured for each fluid at 277.6 K. A  $(47 \pm 7)\%$  increase over the pure R123 heat flux was achieved with the addition of 1% mass hexane to R123. Similarly, the R123/hexane (99/2) mixture gave a maximum percent heat flux enhancement over pure R123 of  $(29 \pm 7)\%$ . The boiling was filmed with a 16 mm high-speed camera. The observations were used to describe various boiling modes on the GEWA-T<sup>TM</sup> surface. The addition of hexane to pure R123 caused a simultaneous reduction in the bubble diameter and increase in the site density. The increase in site density enhanced the boiling despite the reduction in bubble size. Presumably, the site density enhancement was caused by a layer enriched in hexane at the heat transfer surface. The addition of hexane to R123 also improved natural convection. The natural convection was influenced by the greater thermal conductivity of the excess layer which may have contained 55% mass hexane.

**Keywords:** Building Technology, enhanced heat transfer, additive, R123, pool boiling, GEWA-T<sup>TM</sup>, fluid heating, n-hexane

## TABLE OF CONTENTS

ABSTRACT .....	iii
NOMENCLATURE .....	v
INTRODUCTION .....	1
TEST SURFACE .....	2
APPARATUS .....	2
MEASUREMENTS .....	4
Gewa-T Pool-Boiling .....	7
VISUAL OBSERVATIONS .....	9
ENHANCEMENT MECHANISM SPECULATION .....	12
Boiling Region .....	13
Natural Convection Region .....	15
CONCLUSIONS .....	16
ACKNOWLEDGMENTS .....	17
REFERENCES .....	18
FIGURES .....	21

## NOMENCLATURE

### English Symbols

A	coefficients for Laplace equation
C	molar concentration of the solute
$D_b$	departure bubble diameter (m)
$E_{Tw}$	$u_c$ in the wall temperature (K)
$E_{q''}$	percent $u_c$ in heat flux measurement
k	thermal conductivity (W/m·K)
$L_y$	length of test surface (m)
$q''$	average wall heat flux (W/m <sup>2</sup> )
R	gas constant (8.314 J/K•mol)
$r_c$	radius of cavity mouth (m)
s	estimate of standard deviation
T	temperature (K)
$T_w$	temperature of surface at root of fin (K)
$u_c$	combined standard uncertainty
$u_i$	standard uncertainty
x	test surface coordinate, Fig. 2 (m)
y	test surface coordinate, Fig. 2 (m)

### Greek symbols

$\alpha$	thermal diffusivity (m <sup>2</sup> /s)
$\beta$	contact angle (rad)
$\Gamma$	surface excess concentration of solute
$\delta_t$	thermal boundary layer thickness (m)
$\Delta T$	wall superheat: $T_w - T_{s,s}$ (K)
$\sigma$	surface-tension (kg/m•s <sup>2</sup> )

### Subscripts

1%	R123/hexane (99/1)
2%	R123/hexane (98/2)
i	interface
l	liquid
m	mixture
p	pure R123
s	saturated state, solid surface
v	vapor

### Superscripts

—	average
---	---------



## INTRODUCTION

The cost of manufacturing and/or operating a water chiller could be significantly reduced by improving the boiling performance of 1,1-dichloro-2,2,2-trifluoroethane (R123). Liquid additives can be an economical means of enhancing the boiling performance. Liquid additives could make it possible to reduce manufacturing cost because a chiller would require fewer tubes to meet the same duty. Operating costs of new or existing chillers could be reduced because the additive may improve the efficiency of chillers. Typically, binary mixtures exhibit a boiling performance degradation compared to their pure components (Shock, 1982). Consequently, liquid additives that significantly enhance boiling performance are rare; however, the search for them remains worthwhile. Following is a brief history of the search for the additive discussed in this paper.

After a visit to the National Institute of Standards and Technology (NIST) in 1992, Dr. G. S. Shealy<sup>1</sup> approached the author to study an idea that was partially inspired by a NIST publication (later published as Kedzierski (1993)) and data from a publication then in progress (Kedzierski and Kaul, 1993). The NIST work showed that R123 nucleate flow boiling was enhanced with the addition of a small percentage of a low viscosity alkylbenzene lubricant. Lunger and Shealy (1994) were working on attaining an international patent on azeotrope-like compositions of refrigerant/hydrocarbon mixtures. Shealy was interested in applications for the new azeotropes. One of the proposed azeotropes was a mixture of R123 and n-hexane. Shealy believed that because hexane has a low vapor pressure compared to R123, it might behave as a lubricant in R123 and possibly enhance the boiling heat transfer. Shealy's idea worked. This publication presents the heat transfer data that was used to file international patent WO 94/18282.

Most of the work on liquid additives has been in surfactants for aqueous solutions (Jontz and Myers (1960), Shah and Darby (1973) and Wu et al. (1995)). Carey (1992) and Rosen (1978) describe how surfactants reduce the surface-tension of water. Basically, the surfactant molecule must have polar and

---

<sup>1</sup>At the time, G. S. Shealy was a Senior Engineer at the Fluorochemicals Laboratory of E.I. Du Pont De Nemours and Company, Wilmington, DE.

nonpolar ends, i.e., an amphipathic structure. The nonpolar end of the surfactant distorts the interior structure of the solution. The structural distortion requires less work to bring a surfactant molecule to the liquid-vapor interface than is required to bring a water molecule to the surface. By definition, the surface-tension of the liquid-vapor interface is lowered when less work is required to bring a molecule to the surface.

Not much research has been done in surfactants for refrigerants. Aqueous surfactant solutions are relatively common because the surface-tension of water is greater than that of many liquids with amphipathic structures. Typically, the surface-tension of refrigerants is lower than that of amphipathic liquids. Consequently, it is difficult to find a surfactant to lower the liquid-vapor surface-tension of a refrigerant. In fact, the surfactant reported here does not lower the surface-tension of the liquid-vapor interface. Rather, the present surfactant lowers the surface-tension of the solid-liquid interface.

## TEST SURFACE

Figure 1 shows the oxygen-free high-conductivity (OFHC) copper GEWA-T<sup>TM</sup> test plate and thermocouple coordinate system used in this study. Commercially, the GEWA-T<sup>TM</sup> or "T-fin" surface is formed by flattening the tips of the GEWA-K<sup>TM</sup> surface. The GEWA-T<sup>TM</sup> surface in this study was machined directly onto the top of the test plate by electric discharge machining (EDM). Figure 2 shows a photograph of the fin surface. The gap between the fin-tips was 0.348 mm. The surface had approximately 667 fins per meter oriented along the short axis of the plate. The fin-tip width and the fin-height were 1.05 mm and 1.038 mm, respectively.

## APPARATUS

Figure 3 shows a schematic of the apparatus used to measure the pool boiling data of this study. The apparatus was used to measure the liquid saturation temperature ( $T_s$ ), the average pool-boiling heat flux ( $q''$ ), and the wall temperature ( $T_w$ ). The standard uncertainty ( $u_i$ ) is the positive square root of the estimated variance  $u_i^2$ . The combined standard uncertainty ( $u_c$ ) is commonly referred to as the law of



propagation of uncertainty. All measurement uncertainties are reported for a 95% confidence interval.

The three principal components of the apparatus were: test chamber, condenser, and reservoir. The internal dimensions of the test chamber were 25.4 mm X 257 mm X 1.54 m. The test chamber was charged with approximately 7 kg of R123 from the reservoir, giving a liquid height of approximately 80 mm above the test surface. The bottom of the test section, as shown in Fig. 3, was heated with high velocity (2.5 m/s) water flow. The vapor produced by liquid boiling on the test surface was condensed by the brine-cooled, shell-and-tube condenser and returned as liquid to the pool by gravity.

As shown in Fig. 3, the test section was visible through two opposing, flat 150 mm x 200 mm quartz windows. A high-speed camera was used to film the boiling at 1000, 3000, and 6000 frames per second (fps). Two 500 W forward lights illuminated the specimens during filming. Films were taken at selected heat fluxes immediately after the measurement of the heat-transfer coefficient to ensure that the heat from the lights did not influence the measurement.

Several precautions were taken to reduce the errors associated with the liquid saturation temperature measurement. The saturation temperature of the liquid was measured with a 450 mm long 1.6 mm diameter stainless steel sheathed thermocouple. The small diameter provided for a relatively rapid response time. Nearly the entire length of the thermocouple was in contact with either the test refrigerant vapor or liquid to minimize conduction errors. The tip of the thermocouple was placed approximately 2 mm above and 200 mm to the left of the top of the test surface. This placement ensured that approximately 80 mm of the probe length was in a relatively well-mixed portion of the liquid pool. To provide for a saturated liquid pool state, the mass of liquid in the pool was large compared to mass of liquid condensed. At the highest heat flux, it would require nearly one hour to evaporate and condense the entire test chamber charge. Convection and radiation errors were minimal due to low (277.6 K), uniform temperatures attributed to well-insulated, low emissivity, 38 mm aluminum test chamber walls.

The thermocouples were calibrated against a standard in the NIST Temperature Group to a residual standard deviation of 0.005 K. Considering the fluctuations in the saturation temperature during the test and the standard uncertainties in the calibration, the  $u_c$  of the average saturation temperature was no greater than 0.04 K. A thermocouple drift of within 0.1 K was determined by recalibrating the thermocouples one year after the tests were completed. Consequently, the  $u_c$  of the temperature measurements was less than 0.1 K. The saturation temperature was also obtained from a pressure transducer measurement with an uncertainty of less than 0.03 kPa. The uncertainty of the saturation temperature from equilibrium data (Morrison and Ward, 1991) for R123 was 0.17 K. Vapor-liquid equilibrium data for the R123/hexane mixtures were obtained from Shealy (1993). An equation of state (Morrison and McLinden, 1985) was used to extend the mixture equilibrium data to the operating conditions and mixture compositions of the test. The saturation temperature obtained from the thermocouple and the pressure measurement always agreed within  $\pm 0.17$  K.

## MEASUREMENTS

Figure 1 shows the coordinate system for the 20 thermocouple wells in the side of the test plate. The wells were 16 mm deep to reduce conduction errors. Using a method given by Eckert and Goldstein (1976), errors due to heat conduction along the thermocouple leads were estimated to be well below 0.01 mK. The origin of the coordinate system was centered on the surface at the root of the fin. Centering the origin in the y-direction improved the accuracy of the wall heat flux and temperature calculations by reducing the number of fitted constants involved in these calculations. The x-coordinate measures the distance normal to the heat transfer surface. The y-coordinate measures the distance perpendicular to the x-coordinate. The thermocouples were arranged in four sets of five aligned in the x-direction. Following a procedure given by Kedzierski and Worthington (1993), the size and arrangement of the thermocouple wells were designed to minimize the errors in the wall temperature and temperature gradient measurement.

The heat flux and the wall temperature were obtained by regressing the measured temperature distribution

of the block to the governing conduction equation. In other words, rather than using the boundary conditions to solve for the interior temperatures, the interior temperatures were used to solve for the boundary conditions following a procedure given in Kedzierski (1995). Two solutions were found: one for pure R123 for heat fluxes below 10 kW/m<sup>2</sup>:

$$T = A_0 + A_1 x + A_2 y \quad (1)$$

and another for R123/hexane mixtures and pure R123 heat fluxes above 10 kW/m<sup>2</sup>:

$$T = A_0 + A_1 x + A_2 y + A_3 (x^2 - y^2) + A_4 y(3x^2 - y^2) \quad (2)$$

Fourier's law and the fitted constants ( $A_0$ ,  $A_1$ , and  $A_3$ ) were used to calculate the average wall heat flux ( $q''$ ) normal to the heat transfer surface for both the first and third order models as:

$$q'' = \left( \frac{1}{L_y} \int_{-\frac{L_y}{2}}^{\frac{L_y}{2}} k \frac{\partial T}{\partial x} dy \right)_{x=0} = \bar{k} A_1 \quad (3)$$

where  $\bar{k}$  is the average thermal conductivity along the surface of the plate, and  $L_y$  is the length of the heat transfer surface as shown in Fig. 1.

The average wall temperature for the first order model is:

$$\bar{T}_w = \left( \frac{1}{L_y} \int_{-\frac{L_y}{2}}^{\frac{L_y}{2}} T dy \right)_{x=0} = A_0 \quad (4)$$

and that for the third order model is:

$$\bar{T}_w = A_0 - \frac{A_3 L_y^2}{12} \quad (5)$$

A particular model was chosen if it produced the smallest uncertainties in the heat flux and wall temperature calculations. In addition, the model must maintain nearly the same residual standard deviation as the model containing the first nine terms of the two-dimensional Laplace equation. For approximately half of the mixture data, the  $A_2$  constant was set to zero to obtain smaller uncertainties in  $q''$  and  $T_w$ .

Siu et al. (1976) estimated the uncertainty in the thermal conductivity of OFHC to be about 2% to 3% by comparing round-robin experiments. Because the purity of OFHC copper is high, the variability of its thermal conductivity from batch to batch should be small and closely estimated from a comparison of round-robin experiments. Accordingly, the percent  $u_c$  in the average wall heat flux was calculated assuming a 3%  $u_c$  in the thermal conductivity of the plate. Figure 4 shows the percent  $u_c$  in the average wall heat flux ( $E_{q''}$ ) as a function of  $q''$  for the pure R123 and mixture data. The percent  $u_c$  in  $q''$  was greatest at the lowest heat fluxes, approaching 10% of the measurement at 10 kW/m<sup>2</sup> for pure R123 and R123/hexane (98/2). Moreover, the  $u_c$  R123/hexane (99/1) heat flux approaches 20% of the measurement at 10 kW/m<sup>2</sup>. The  $E_{q''}$  appears to be relatively constant between 6% and 3% for heat fluxes above 30,000 W/m<sup>2</sup>.

Figure 5 shows the  $u_c$  in the temperature of the surface at the root of the fin ( $E_{T_w}$ ) as a function of heat flux for all of the data. The  $u_c$  in  $T_w$  was calculated from the regression of Laplace's equation. The  $u_c$  in the wall temperature for the mixture data was somewhat parabolic with heat flux and fell between 0.08 K and 0.03 K. The average random error in the wall superheat --  $\Delta T_s = \overline{T_w} - T_s$  -- was within 0.1 K.

The combined standard uncertainties shown in Figs. 4 and 5 are "within-run uncertainties." These do not include the uncertainties due to "between-run uncertainties" or differences observed between tests taken on different days. The "within-run uncertainties" include only the random effects and uncertainties evident from one particular test. All other uncertainties are reported as "between-run uncertainties"

which include all random effects such as surface past history or seeding. "Within-run uncertainties" are given only in Figs. 4 and 5.

### Gewa-T Pool-Boiling

The heat flux was varied from  $10 \text{ kW/m}^2$  to  $80 \text{ kW/m}^2$  to simulate typical operating conditions of R123 chillers equipped with enhanced tubes. All evaporation tests were taken at  $277.6 \text{ K}$ . The data were recorded consecutively starting at approximately  $74 \text{ kW/m}^2$ , increasing up to  $80 \text{ kW/m}^2$ , and then descending to  $20 \text{ kW/m}^2$ . The descending heat flux procedure minimized the possibility of any hysteresis effects on the data which would have made the data sensitive to the initial operating conditions.

The mixtures were prepared by charging measured weights of R123 and spectrophotometric grade hexane into an evacuated reservoir (see Fig. 3). All compositions are given on a mass percent basis. The liquid was injected into a drop tube that nearly touched the bottom of the reservoir. First, approximately 90% of the R123 was charged. Then the hexane was injected with a syringe through the drop tube, followed by flushing with the remaining R123 charge. The flushing of R123 through the drop tube also assisted in mixing the sample. The amount of R123 that remained in the drop tube after flushing had a negligible effect on the composition. The heat-transfer test chamber was charged with the test fluid from this reservoir.

Three compositions were investigated: (1) pure R123, (2) R123/hexane (99/1), and (3) R123/hexane (98/2). Figures 6 through 8 are plots of the measured heat flux ( $q$ ) versus the measured wall superheat ( $T_w - T_s$ ). The pure R123, the R123/hexane (99/1), and the R123/hexane (98/2) data were taken on four, five and two days, respectively. The solid line is a best-fit regression or estimated mean of the data. The dashed lines to either side of the mean represent the lower and upper 95% simultaneous (multiple-use) confidence intervals for the mean. The  $u_c$  of the estimated mean wall superheat in the natural convection region and the boiling region is approximately  $0.1 \text{ K}$  and  $0.07 \text{ K}$ , respectively. The figures illustrate that, depending upon the operating condition and composition, R123/hexane mixtures exhibited

a heat transfer enhancement compared to pure R123.

Figure 6 presents the boiling curve for pure R123 at 277.6 K on the GEWA-T surface. The boiling curve exhibits two characteristic regimes: a natural convection regime and a nucleate boiling regime. The regimes are separated by the cessation of nucleate boiling (CNB). A well-defined CNB occurs for the pure R123 data at approximately 7.6 K. The nucleate boiling regime exists for superheats greater than the CNB condition. Here, the heat transfer is governed primarily by the formation of isolated bubbles within the fin cavities. For superheats below the CNB, the influence of natural convection becomes prevalent. In fact, pure R123 bubble generation was not visible on the heat transfer surface in the natural convection regime with the exception of the vicinity of the CNB.

Figure 7 compares the R123/hexane (99/1) boiling data to the mean of the R123 data. The addition of 1% mass hexane to R123 has improved the boiling performance in two ways: (1) the average R123/hexane (99/1) mixture heat flux is approximately 24% above that of pure R123 for heat fluxes from 8 kW/m<sup>2</sup> to 73 kW/m<sup>2</sup>, and (2) the 99/1 mixture boils at superheats smaller than the CNB of pure R123. Lower superheats required for boiling permit evaporators to operate at lower approach temperature differences which leads to more efficient operation of refrigeration equipment. Higher heat fluxes could be used to either reduce the required size of the evaporator or to improve the efficiency of existing refrigeration equipment.

Figure 8 shows that a doubling of the hexane concentration results in an average heat flux degradation of 5% over the range of 10 kW/m<sup>2</sup> to 80 kW/m<sup>2</sup>. Essentially, only natural convection and low heat flux boiling heat transfer are enhanced. A heat transfer degradation occurs at heat fluxes above 34 kW/m<sup>2</sup>. The CNB for both the 99/1 and the 98/2 mixtures is not as clearly defined as it is for pure R123. The gradual transition from the boiling to natural convection suggests that boiling does not cease as abruptly for the mixture as it does for the pure R123.

Figure 9 summarizes the effect of the addition of hexane to R123 on the R123 heat flux. The figure plots the ratio of the mixture to the pure R123 heat flux ( $q''_{1\%}/q''_p$  or  $q''_{2\%}/q''_p$ ) versus the pure R123 heat flux ( $q''_p$ ) at the same wall superheat. Notice that the enhancement curves for the two mixtures have similar forms suggesting that a family of curves may exist for various compositions. Both exhibit a maximum at a R123 heat flux of approximately  $23 \text{ kW/m}^2$ . The maximum is probably a result of the cessation of boiling for pure R123 while the mixture boiling continues at  $23 \text{ kW/m}^2$ . At this point, the maximum percent heat flux enhancement is  $(47 \pm 7)\%$  for the 99/1 mixture and  $(29 \pm 7)\%$  for the 98/2 mixture. An average enhancement of 19 % exists from  $10 \text{ kW/m}^2$  to  $33.5 \text{ kW/m}^2$  for the 98/2 mixture. The average enhancement is consistent with a 13 % to 20% increase in the evaporation heat transfer coefficient with the addition of 1 % mass n-Pentane to R123 which was measured by the Trane Company (Glamm, 1995). The mean enhancement for the 99/1 mixture never dropped below 5% for all test conditions. By contrast, the 98/2 mixture exhibited an average degradation of 18% within the range of  $33.5 \text{ kW/m}^2$  to  $80 \text{ kW/m}^2$ .

Figures 10 and 11 provide 95% simultaneous confidence intervals for the enhancement ratios for the 99/1 and 98/2 mixtures, respectively. Because the confidence intervals for the 99/1 mixture are both above the value one, an enhancement exists for all of the heat fluxes tested for 95% confidence. Figure 11 shows that a degradation exists for the 98/2 mixture for heat fluxes above  $45 \text{ kW/m}^2$ .

## VISUAL OBSERVATIONS

Figures 12 through 17 show schematics of the bubble activity within the cavities of the Gewa-T surface. A comparison of the figures illustrates that the enhancement mechanism is similar to that caused by lubricants as described in Kedzierski (1992) and Kedzierski and Kaul (1993). The addition of hexane to pure R123 causes a simultaneous reduction in the bubble diameter and increase in the site density. Tzan and Yang (1990) also observed this same trend for surfactants in aqueous solutions.

Figures 12 through 17 are schematics of the bubble activity for the three test fluids at two different heat

fluxes. Figure 12 depicts the three different boiling modes for R123 at  $q'' = 70 \text{ kW/m}^2$ . Each mode depends on the size of the bubble as it exists when it is in the cavity. The bubble modes for small, large (mushroom), and intermediate size bubbles are illustrated from left to right in Figure 12.

The small cavity-bubble formation mode occurs when small diameter bubbles are individually formed and travel unobstructed through the gap between the fins. The small bubble formation mode dominated approximately 70% of the bubble formation occurrences. The bubbles were approximately 0.26 mm to 0.32 mm in diameter.

Figure 13 depicts the sequence of events that describe the large cavity-bubble mode. First, several small bubbles are almost simultaneously formed. If the bubbles are sufficiently congested within the cavity, they will coalesce into one large bubble. Due to the close proximity of the bubble to the cavity walls, the bubble quickly picks up energy from the superheated liquid and ejects vapor through the fin gap, while maintaining a vapor root within the cavity. When the buoyancy force on the portion of the bubble above the fins is large enough, it will cause the vapor root to be pulled out of the cavity.

Figure 16 illustrates the bubble formation mode for intermediate size bubbles. This mode occurs when a cavity bubble is larger than the gap between the fins, but not large enough to get close to the superheated liquid layer to grow rapidly. The bubble is retained by the fin tips. It receives energy directly from the corners of the fin and grows until buoyancy forces pull the bubble from the fin. The last two boiling modes are advantageous since they efficiently create additional vapor. That is, vapor is generated when the bubble is large and the surface-tension forces are more easily overcome. The intermediate and large cavity-bubble modes occurred at about equal frequencies and together contributed to 30% of the bubble activity.

Figure 13 shows that more sites were active for the R123/hexane (99/1) mixture than for pure R123. The cavity bubbles were smaller, but more numerous. Also, 0.1 mm diameter bubbles generated on the



tops of the fins were visible for the R123/hexane (99/1) mixture, but were not visible for pure R123 nor the 98/2 mixture. The bubble activity was approximately split between the large and small bubble modes. The intermediate bubble mode appeared to be absent for the 99/1 mixture. In general, the R123/hexane (99/1) mixture exhibited more smaller diameter bubbles (0.2 mm) than pure R123 exhibited. Consequently, because a greater number of small bubbles increases the probability of coalescence, the 99/1 mixture also exhibited more large mushroom cavity-bubbles. The addition of hexane caused more sites to become active. This enhanced the heat transfer directly by producing more vapor through a greater number of individual bubbles, and it caused the increase in the occurrence of the mushroom bubble mode, which is a more efficient mode of vaporization.

Figure 14 shows that fewer sites were active for the R123/hexane (98/2) mixture than for the 99/1 mixture. As compared to the 99/1 mixture bubbles, the 98/2 mixture bubbles were marginally smaller (0.18 mm) and were less numerous. Also, no 98/2 mixture bubbles were generated on the tops of the fins. The mushroom bubbles dominated the bubble activity; however, instead of originating from coalesced bubbles, the mushroom bubbles grew directly from the side of the cavity wall.

A summary of representative bubble characteristics at  $70 \text{ kW/m}^2$  is given below. The individual frequency for the small bubbles and the mushroom bubbles was nearly the same for the three fluids tested: approximately 340 bubbles/sec and 75 bubbles/seconds, respectively. The R123/hexane (99/1) mixture produced approximately 70% more bubbles than the pure R123. Approximate values for the site density per channel are: 22,000 sites/ $\text{m}^2$ , and 13,000 sites/ $\text{m}^2$  for the R123/hexane (99/1) and the pure R123, respectively. The site density of R123/hexane (99/2) was approximately 17,000 sites/ $\text{m}^2$ . These are only representative values obtained from averaging the available data. A wide range of bubble frequencies and site density existed for each fluid.

Figures 15 through 17 are schematics of the bubble activity for the three test fluids at  $q'' = 30 \text{ kW/m}^2$ . Natural convection density gradients or Schlieren were visible over the entire surface for all test fluids.

Most of the heat transfer surface was inactive with the exception of a few sparse sites. Mushroom bubbles were not present. The R123/hexane (99/1) appeared to have the most bubble activity of the fluids at 30 kW/m<sup>2</sup>. R123 and the 98/2 mixture had similar bubble activities at 30 kW/m<sup>2</sup>.

#### ENHANCEMENT MECHANISM SPECULATION

The visual observations have shown that the R123/hexane (99/1) bubbles are smaller and more numerous than those for pure R123. It is reasonable to assume that the boiling heat transfer is enhanced by the increase in the number of bubbles produced despite the reduction in their size. An overall description of the boiling mechanism is given below. Then an explanation is offered for why the mixture bubbles are smaller and more numerous than the pure R123 bubbles.

It is speculated that the pool boiling enhancement mechanism associated with the addition of hexane to R123 is due to an accumulation of hexane at the boiling surface. The excess concentration arises from the relatively low vapor pressure of hexane when compared to R123. The hexane can be drawn out of solution as a consequence of refrigerant evaporation. The R123/hexane liquid mixture travels to the heated wall, and the R123 preferentially evaporates from the surface leaving behind a liquid phase enriched in hexane. A balance between deposition and removal of the hexane establishes some unknown excess concentration of hexane at the surface. In summary, preferential evaporation of the refrigerant presumably creates a thin hexane-rich layer on the heated surface.

Indirect experimental evidence for a boiling induced excess layer is the improvement of the heat transfer performance with the duration of the test. At the start of each test day the mixture was boiled at the highest heat flux for approximately three hours to allow the heat transfer performance to increase and level off. The initial performance would approximately reproduce the pure R123 value and increase to that reported here. Apparently, the hexane-rich layer was established during this "break-in" period.

### Boiling region

For R123/hexane mixture boiling, small bubbles arise from small attractive forces between the hexane-rich excess layer and the heat transfer surface. Although less heat transfer occurs with a smaller bubble, the site density can be increased as a direct consequence of the small bubble size. An enhancement of the boiling is achieved if the increase in site density more than compensates for the decrease in bubble size. The next few paragraphs provide a more detailed speculative discussion on the enhancement mechanism for R123/hexane mixture pool boiling.

The R123/hexane bubbles are small due to the existence of the hexane-rich excess layer at the boiling surface. For a surface excess concentration of the solute ( $\Gamma$ ), the Gibbs adsorption equation for a dilute solution (Rosen, 1978) predicts a reduction in the surface-tension between the mixture and the solid surface:

$$d\sigma = -RT_i \Gamma d\ln C$$

where  $R$  is the gas constant,  $T_i$  is the temperature of the interface, and  $C$  is the molar concentration of the solute. If the concentration of the solute (hexane) is increased above the bulk concentration ( $\Gamma \neq 0$ ), then the surface-tension ( $\sigma$ ) between interfacing materials will be lower (negative sign in Gibbs eqn.) than what it would have been if the interface concentration was at the bulk composition. A reduction in the surface-tension between a liquid and a boiling surface will induce a corresponding reduction in the size of the departing bubbles. The surface-tension between the liquid and the solid ( $\sigma_{ls}$ ) determines the magnitude of the bubble attachment force by establishing the magnitude of the contact angle ( $\beta$ ). This can be demonstrated with the use of the Young and Dupré equation (Adamson, 1967) which is a lateral force balance on a bubble attached to a surface:

$$\beta = \arccos \left( \frac{\sigma_{vs} - \sigma_{ls}}{\sigma_{lv}} \right) \quad (7)$$

For fixed surface tension between the liquid and the vapor ( $\sigma_{lv}$ ) and the vapor and the solid ( $\sigma_{vs}$ ), a reduction in  $\sigma_{ls}$  causes a reduction in the contact angle  $\beta$ . The bubble is held to the wall by a surface

tension force proportional to  $\sigma_{lv}\sin\beta$ . The size of the bubble determines the buoyancy forces on the bubble acting to detach the bubble. A smaller contact angle induces a small bubble attachment force and consequently, a small bubble size. Accordingly, the mixture bubbles are smaller than the pure R123 bubbles.

Heuristically, the bubble grows within/on the excess layer, rather than on the copper surface. In the limit, if a bubble were to grow solely on the hexane-rich layer, the attachment force would be negligible compared to the attachment force for a bubble growing on a solid surface. The small attachment force arises from the small difference between the surface-tensions of R123 and the hexane-rich layer (boiling surface). Consequently, the bubble does not hold to the hexane rich surface as strongly as it does to the copper surface. As a result, the R123/hexane bubbles are smaller than the pure R123 bubbles.

Hsu's (1962) model can be used to show that smaller bubbles will induce higher site densities than larger bubbles. Figure 18 schematically illustrates the proposed site enhancement mechanism by comparing the growth of R123/hexane and R123 bubbles in identical conical cavities. Both bubbles originate below the thermal boundary layer thickness ( $\delta_t$ ) which exists as a thin layer near the heated surface where  $T > T_s$ . According to Hsu's (1962) model, a site will be active if the bubble is released from the wall before it grows beyond the thermal boundary layer. A bubble that grows beyond  $\delta_t$  while attached to the wall condenses and causes the site to be inactive. For a given cavity distribution, more of the larger cavities will be active for the mixture than for the pure R123.

It was implied that the thermal boundary layers for the mixture and pure R123 were equal in the above argument. However, the thermal properties of the excess layer differ from those of R123. An estimate of the ratio of the R123 to the mixture thermal boundary layer thickness was derived from the model of Bosnjakovic (1930):

Assuming a 55% hexane excess layer, the R123/hexane (99/1) thermal boundary layer thickness is 12%

$$\frac{\delta_{t_m}}{\delta_{t_p}} = \sqrt{\frac{\alpha_m}{\alpha_p}} \quad (8)$$

larger than pure R123. Although, a thicker thermal boundary layer would tend to allow more sites to be active, the primary site enhancement mechanism is probably induced by small bubbles.

An increase in the number of active sites is also induced in another way by the smaller bubble size. Westwater (1956) shows that the probability of bubble nucleation increases when less work is required to form a bubble. Less work is required to form small bubbles than large bubbles. The increase in site density for small bubbles is probably due to the coupled effects of lower bubble formation work and the bubble's growth within the thermal boundary layer.

The cause of the enhancement mechanism associated with a dilute solution of hexane in R123 is different from that observed for surfactants in aqueous solutions. Surfactants in water lower the surface-tension of the liquid-vapor interface. In contrast, the hexane lowers the surface-tension of the liquid-solid interface. There are two reasons why hexane cannot lower the liquid-vapor interface surface-tension of R123. First, the surface-tension of hexane is larger than that of R123, so the hexane is repelled from the liquid-vapor interface. Second, a surfactant must have a polar end (a lyophilic group) that is attracted to the polar solvent to establish a stable liquid-vapor interface structure. Hexane has a zero dipole moment. Therefore, hexane does not have the characteristic molecular structure of a surfactant.

#### Natural Convection Region

The enhancement of the heat flux in the natural convection region could also be a consequence of the excess concentration of hexane at the heat transfer surface. At 277.6 K, hexane has a higher thermal conductivity (122 mW/m-K) than R123 (80 mW/m-K). Consequently, natural convection improves for mixtures of R123 and hexane with increasing concentrations of hexane. The local concentration of hexane at the surface (assuming a linear mixing rule) would have to be 52% and 80% by mass to achieve, respectively, a 20% and 30% enhancement due to an increase in thermal conductivity. Given a bulk

concentration of 1% hexane, an excess concentration of 52% and 80% hexane at the heat transfer surface is large but possible.

The natural convection enhancement described above is supported by an excess concentration at the test surface. As a result, the enhancement should be temporary. The boiling process drives the hexane to the surface and maintains an excess concentration there. In the absence of boiling, there is no driving force to hold the hexane to the surface. Consequently, the natural convection will drive the hexane from the surface since its density is less than half that of R123. Unfortunately, no tests were conducted to validate this hypothesis. On the other hand, there is some support for this theory based on the degradation of the natural convection enhancement with descending heat flux (increasing time). For example, if the enhancement is due to increased thermal conductivity, it should follow the concentration at the surface. A higher concentration at the surface would produce a greater enhancement. A constant concentration would induce a constant enhancement. Accordingly, because the enhancement mostly degrades as time progresses (descending heat flux), this could indicate that the hexane is being transported from the surface and consequently simultaneously lowering the local thermal conductivity of the liquid mixture at the surface and the enhancement of the heat flux.

## CONCLUSIONS

The pool boiling performance of R123 on a GEWA-T<sup>TM</sup> surface was enhanced as much as  $(47 \pm 7)\%$  by adding 1% mass hexane. The maximum percent heat flux enhancement for R123/hexane (99/2) mixture was  $(29 \pm 7)\%$ . Observations from high-speed 16 mm films of the boiling revealed that the addition of hexane to pure R123 causes a simultaneous reduction in the bubble diameter and an increase in the site density. The pool boiling enhancement mechanism is presumably due to an accumulation of hexane at the boiling surface. The excess layer reduces the surface-tension between the liquid and the heat transfer surface causing the production of small diameter bubbles. Smaller bubbles will induce higher site densities than larger bubbles. The site density is increased enough to more than compensate for the loss in bubble size and result in a net heat transfer enhancement. The addition of hexane to R123

also improves natural convection. The natural convection is influenced by the greater thermal conductivity of the hexane enriched excess layer.

#### **ACKNOWLEDGEMENTS**

This work was jointly funded by NIST, Dupont, and the U.S. Department of Energy (project no. DE-01-95CE23808.000 modification #A004) under Project Managers Glenn Shealy and Bill Noel, respectively. Thanks goes to the following NIST personnel for their constructive criticism of the first draft of the manuscript: Dr. D. A. Didion, Dr. M. O. McLinden, Mr. P. I. Rothfleisch, and Mrs. J. Land. The author would also like to express appreciation to E. Bellinger and A. Dashottar for data collection. Furthermore, the author extends appreciation to Dr. E. Lagergren for consultations on the uncertainty analysis.

## REFERENCES

- Adamson, A. W., 1967, Physical Chemistry of Surfaces, Interscience Publ., New York, 2nd Ed., p. 353.
- Carey, V. P., 1992, Liquid-Vapor Phase-Change Phenomena, Hemisphere, Washington.
- Eckert, E. R. G., and Goldstein, R. J., 1976, Measurements in Heat Transfer, Hemisphere, Washington, 2nd ed., pp. 9-11.
- Glaum, P., 1995, Private communications, The Trane Company, La Crosse, Wisconsin.
- Hsu, Y. Y., 1962, "On the Size Range of Active Nucleation Cavities on a Heating Surface," J. Heat Transfer, Vol. 84, pp. 207-216.
- Jontz, P. D., and Myers, J. E., 1960, "The Effect of Dynamic Surface Tension on Nucleate Boiling Coefficients," AIChE Journal, Vol. 6, No. 1. pp. 34-38.
- Kedzierski, M. A., 1995, "Calorimetric and Visual Measurements of R123 Pool Boiling on Four Enhanced Surfaces," NISTIR 5732, U.S. Department of Commerce, Washington.
- Kedzierski, M. A., 1993, "Simultaneous Visual and Calorimetric Measurements of R11, R123, and R123/Alkylbenzene Nucleate Flow Boiling," Heat Transfer with Alternative Refrigerants, ASME HTD-Vol. 243, H.J. Sauer, Jr. and T.H. Kuehn, Eds., ASME, New York, pp. 27-33.
- Kedzierski, M. A., and Kaul, M. P., 1993, "Horizontal Nucleate Flow Boiling Heat-transfer-coefficient



Measurements and Visual Observations for R12, R123, and R123/Ester Lubricant Mixtures," 6th Int. Symp. on Transport Phenomena in Thermal Engineering, Seoul, Korea, vol. I, pp. 111-116.

Kedzierski, M. A., and Worthington, J. L. III, 1993, "Design and Machining of Copper Specimens with Micro Holes for Accurate Heat Transfer Measurements," Experimental Heat Transfer, vol. 6. pp. 329-344.

Lunger, B. S., and Shealy, G. S., 1994, "Compositions of a Hydrofluorocarbon and a Hydrocarbon," International Patent WO 94/18282.

Morrison, G. and McLinden, M.O., 1985, "Application of a Hard Sphere Equation of State to Refrigerants and Refrigerant Mixtures," NBS Technical Note 1226, National Bureau of Standards, Gaithersburg, MD.

Morrison, G, and Ward, D. K., 1991, "Thermodynamic Properties of Two Alternative Refrigerants: 1,1-Dichloro-2,2,2-Trifluoroethane (R123) and 1,1,1,2-Tetrafluoroethane (R134a)," Fluid Phase Equilibria, Vol 62, pp. 65-86.

Rosen, M. J., Surfactants and Interfacial Phenomena, John Wiley & Sons, New York, p.57.

Shah, B. H., and Darby, R., 1973, "The Effect of Surfactant on Evaporative Heat Transfer in Vertical Film Flow," Int. J. Heat Mass Transfer, Vol. 16, pp. 1889-1903.

Shealy, G. S., 1993, Private communications, Du Pont Chemicals, Wilmington, Delaware.

Shock, R. A. W., 1982, "Boiling in Multicomponent Fluids," Multiphase Science and Technology, Hemisphere Publishing Corp, Vol. 1, pp. 281-386.

Siu, M. C. I., Carroll, W. L., and Watson, T. W., 1976, "Thermal Conductivity and Electrical Resistivity of Six Copper-Base Alloys," NBSIR 76-1003, U.S. Department of Commerce, Washington.

Tzan, Y. L., and Yang, Y. M., 1990, "Experimental Study of Surfactant Effects on Pool Boiling Heat Transfer," J. Heat Transfer, Vol. 112, pp. 207-212.

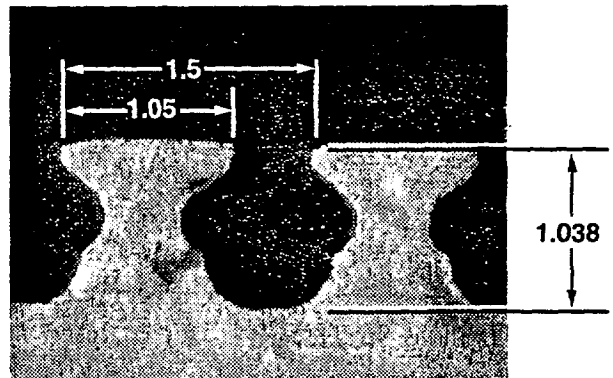
Westwater, J. W., 1956, "Boiling of Liquids," Advances in Chemical Engineering, Vol. 1, T. B. Drew and J. W. Hoopes, Jr., eds., Academic Press, New York.

Wu, W., Yang, Y., and Maa, J., 1995, "Enhancement of Nucleate Boiling Heat Transfer and Depression of Surface Tension by Surfactant Additives," J. Heat Transfer, Vol. 117, pp. 526-529.





**PERSPECTIVE SIDE VIEW**



**SIDE VIEW**

**GEWA-T**

Fig. 2 Photograph of GEWA-T<sup>TM</sup> geometry

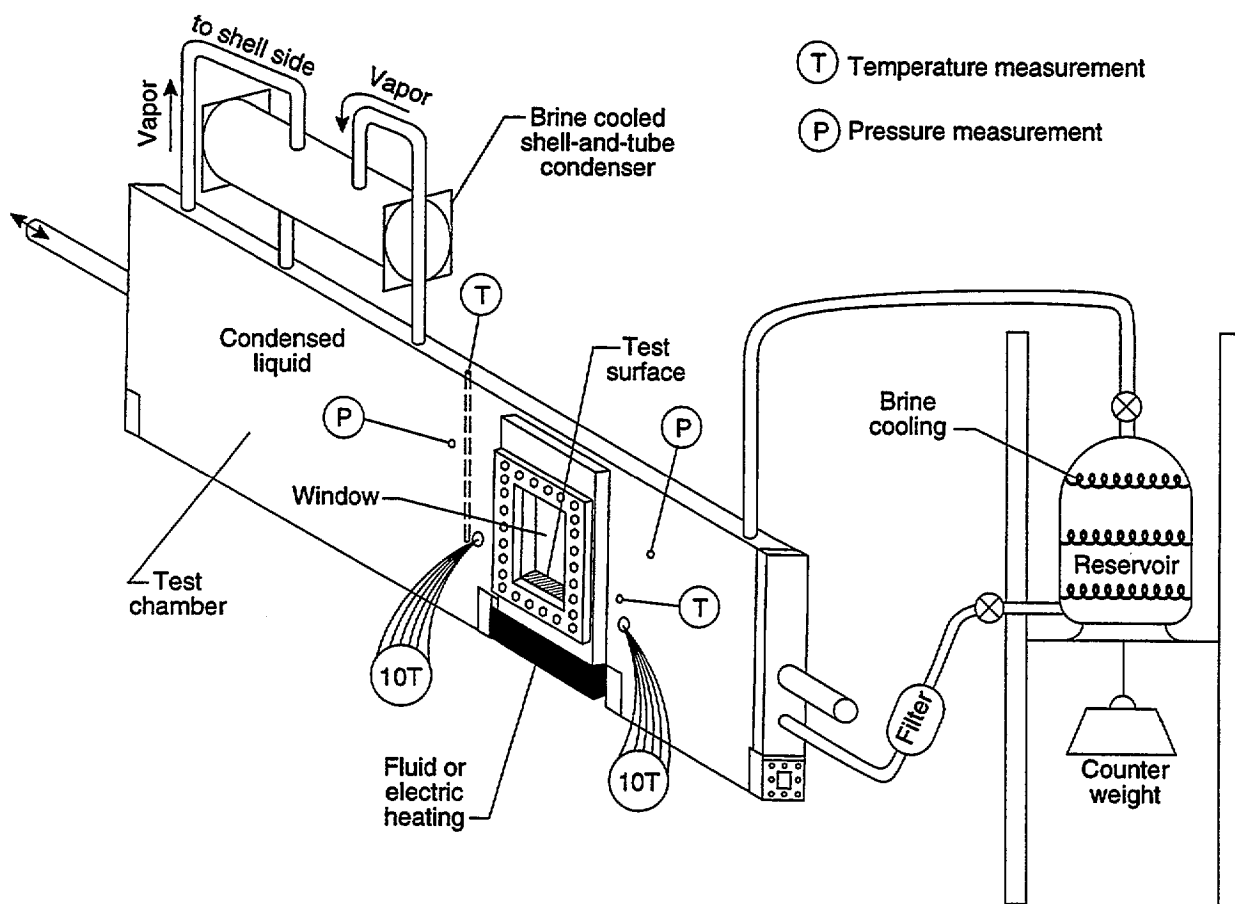


Fig. 3 Schematic of test apparatus

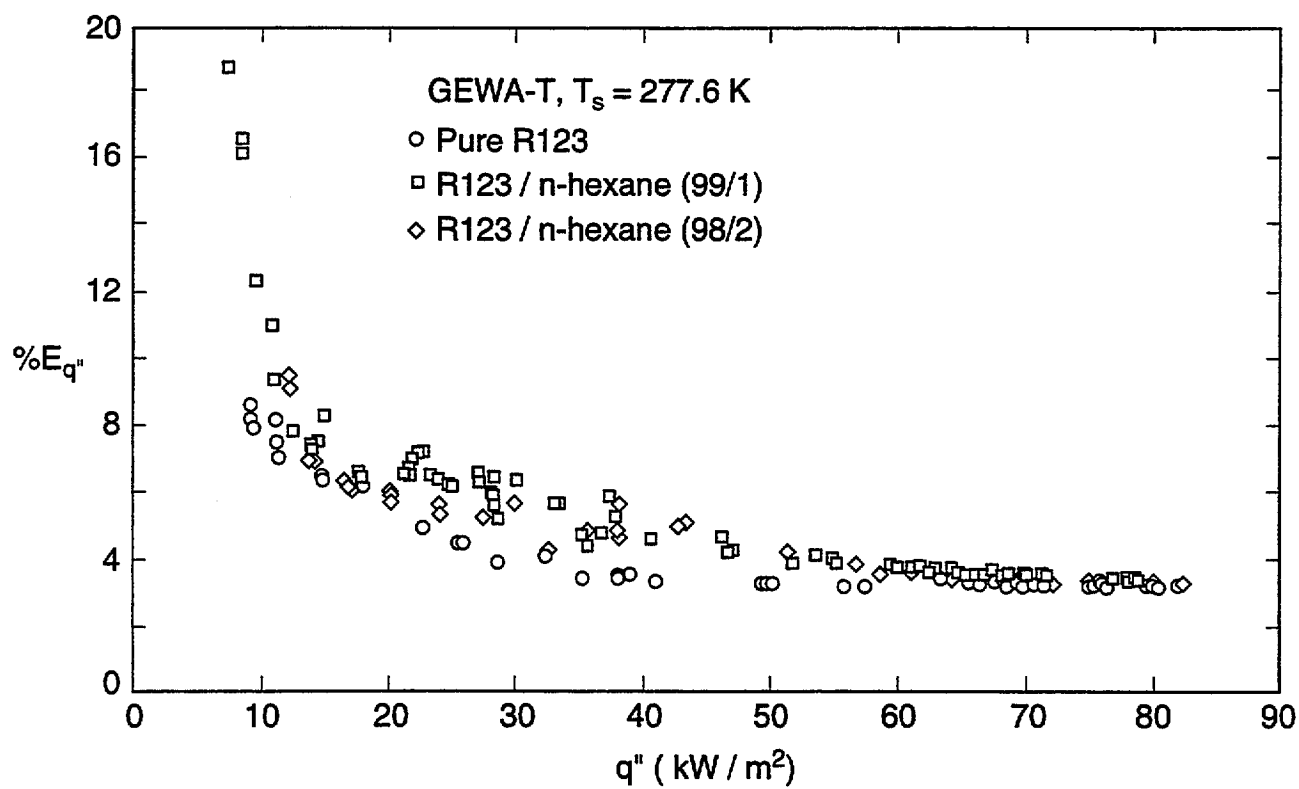


Fig. 4 Percent  $u_c$  in the average wall heat flux

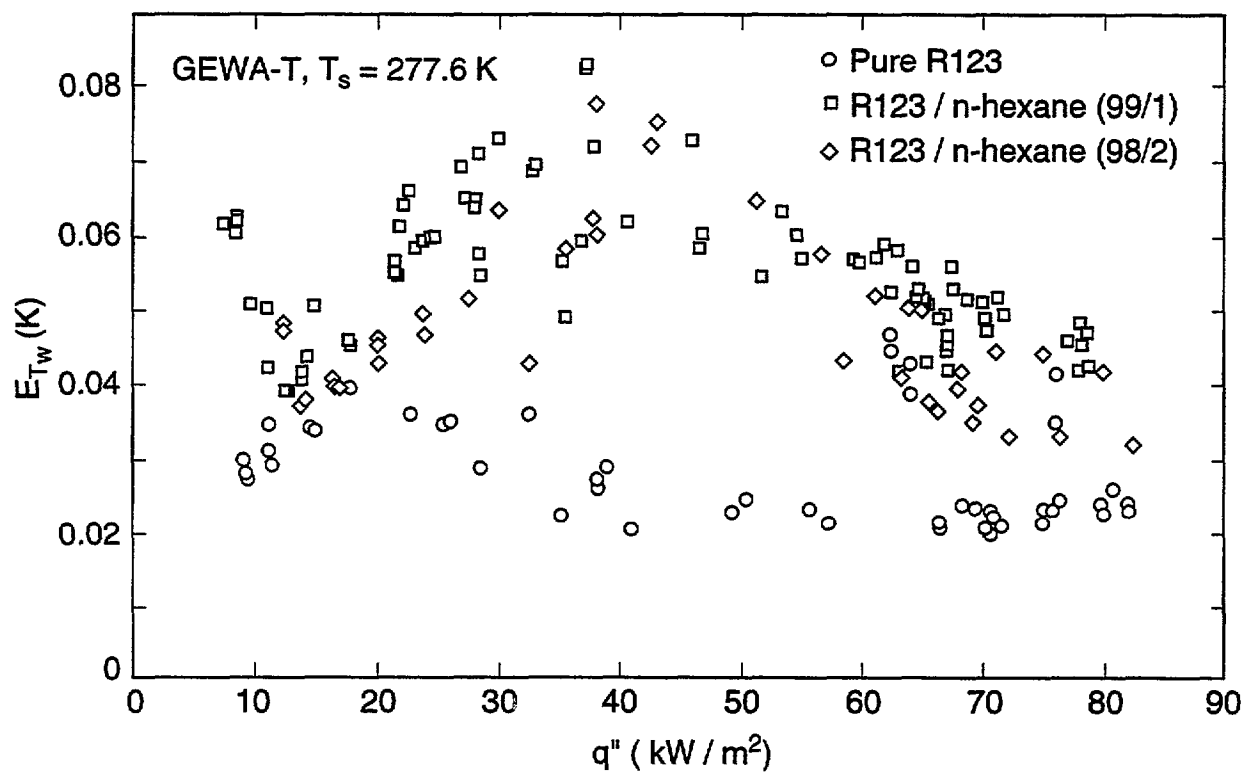


Fig. 5 The  $u_c$  in the temperature at the root of the fin

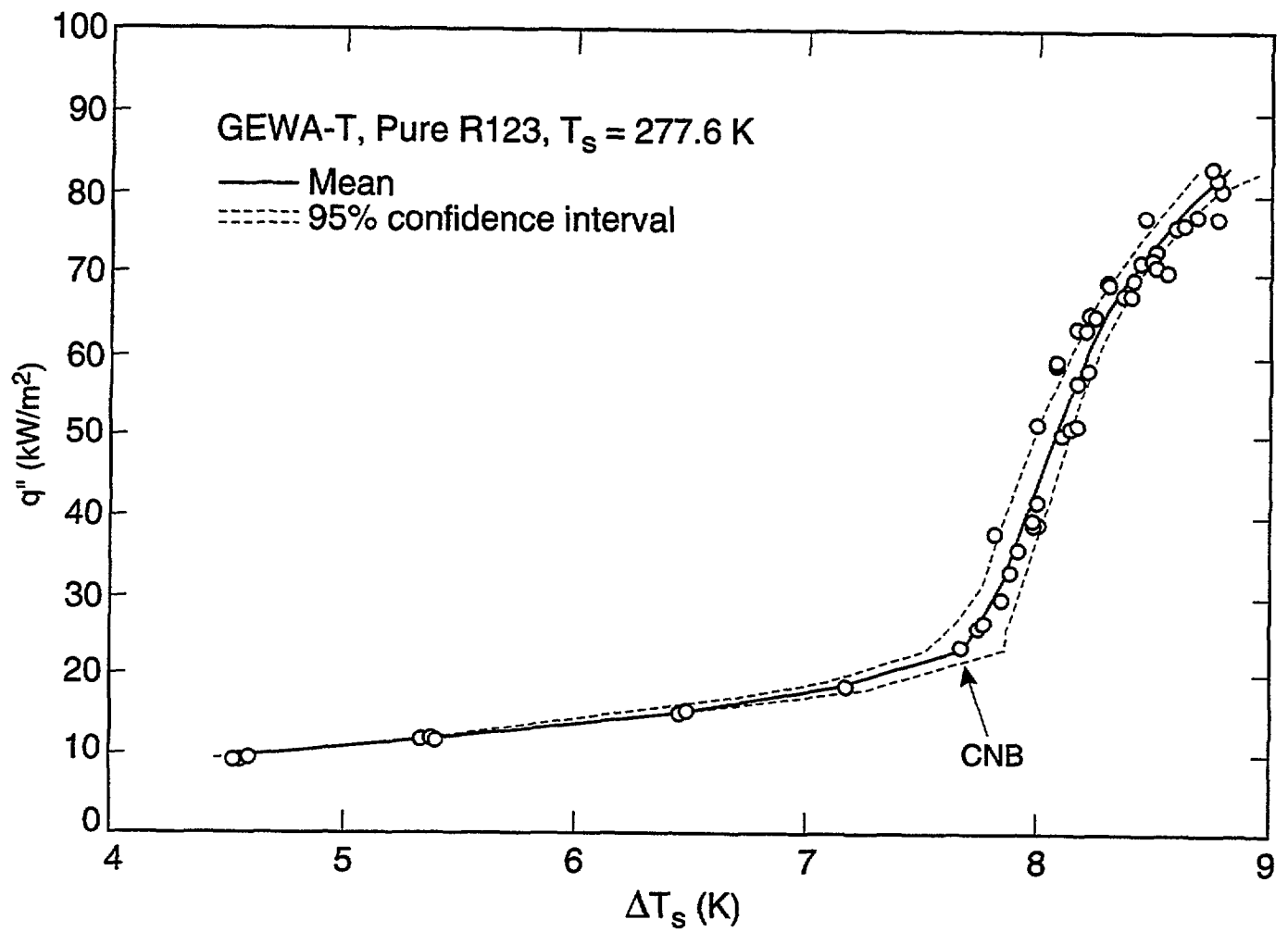


Fig. 6 Boiling curve for pure R123 at 277.6 K on the GEWA-T surface



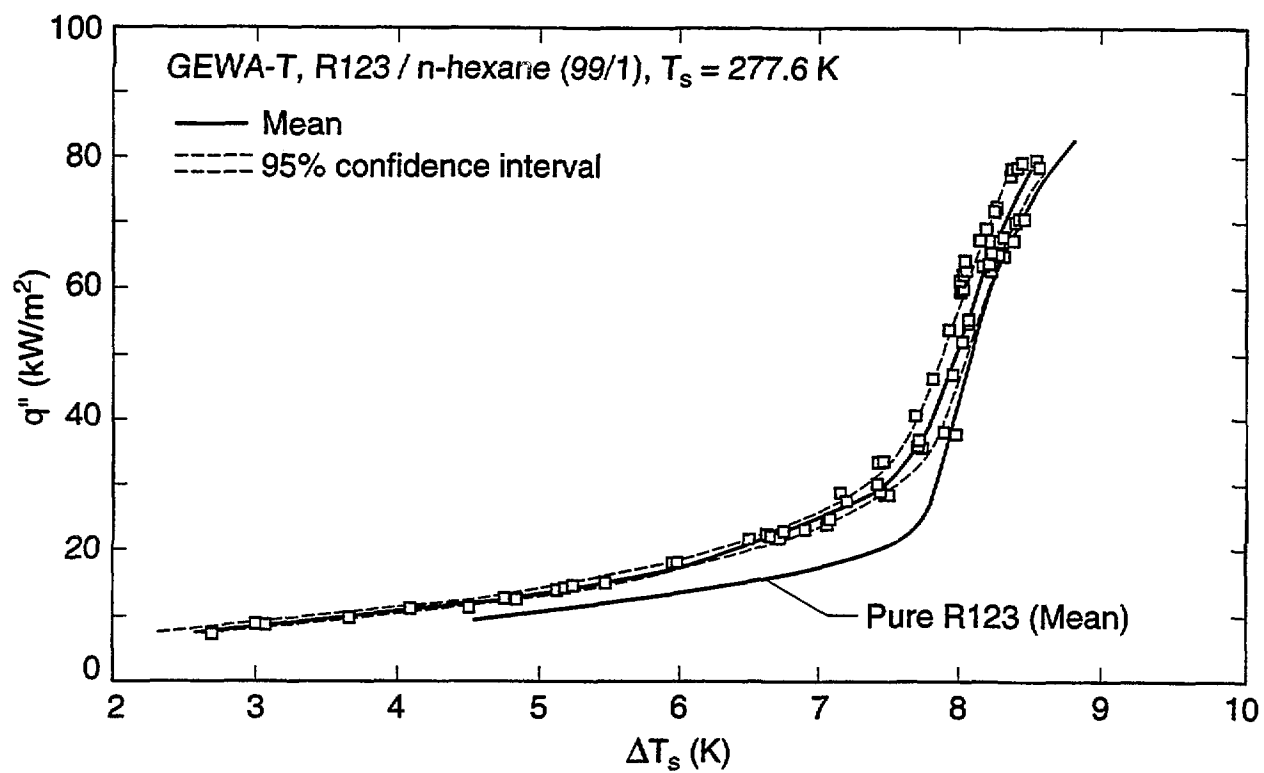


Fig. 7 Comparison of the R123/hexane (99/1) boiling data to the mean of the R123 data

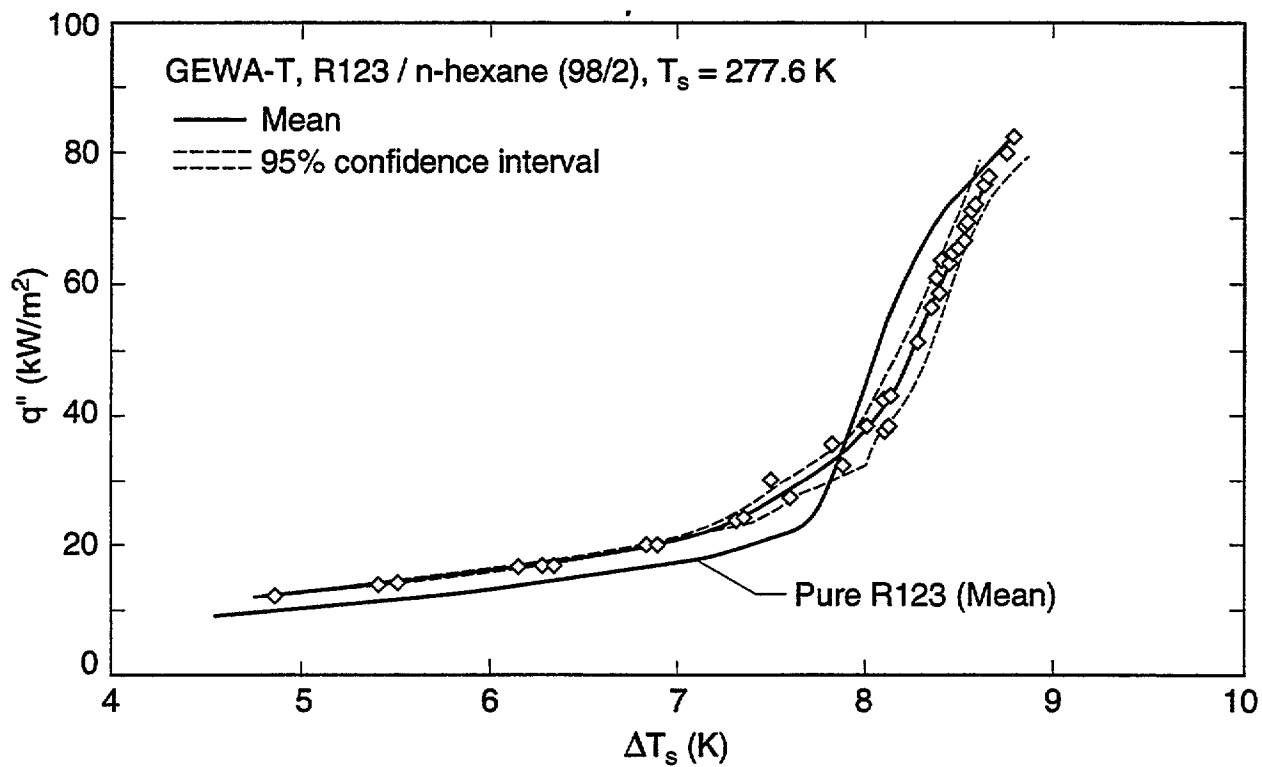


Fig. 8 Comparison of the R123/hexane (98/2) boiling data to the mean of the R123 data

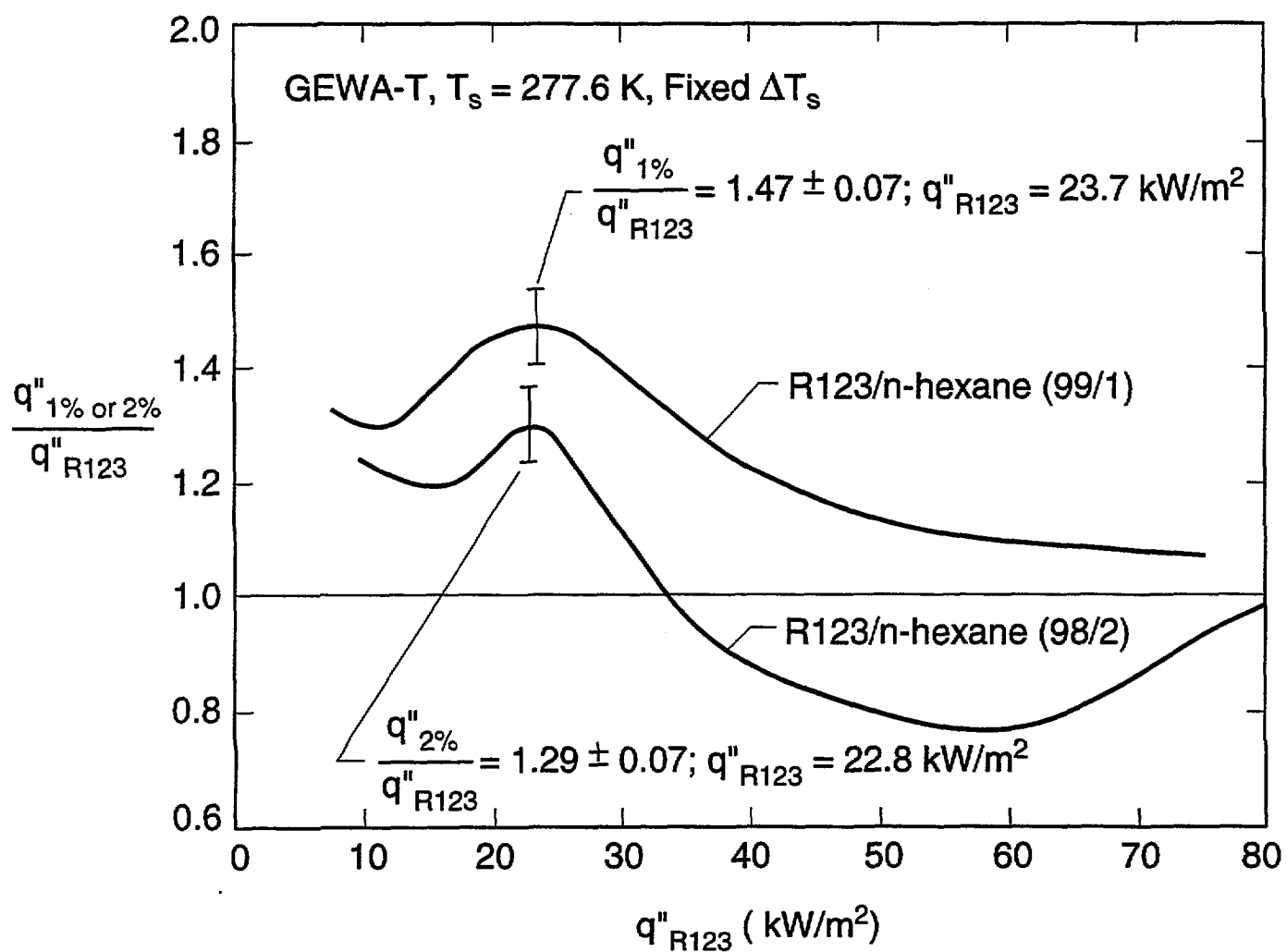


Fig. 9 Effect of hexane on R123 pool boiling heat flux

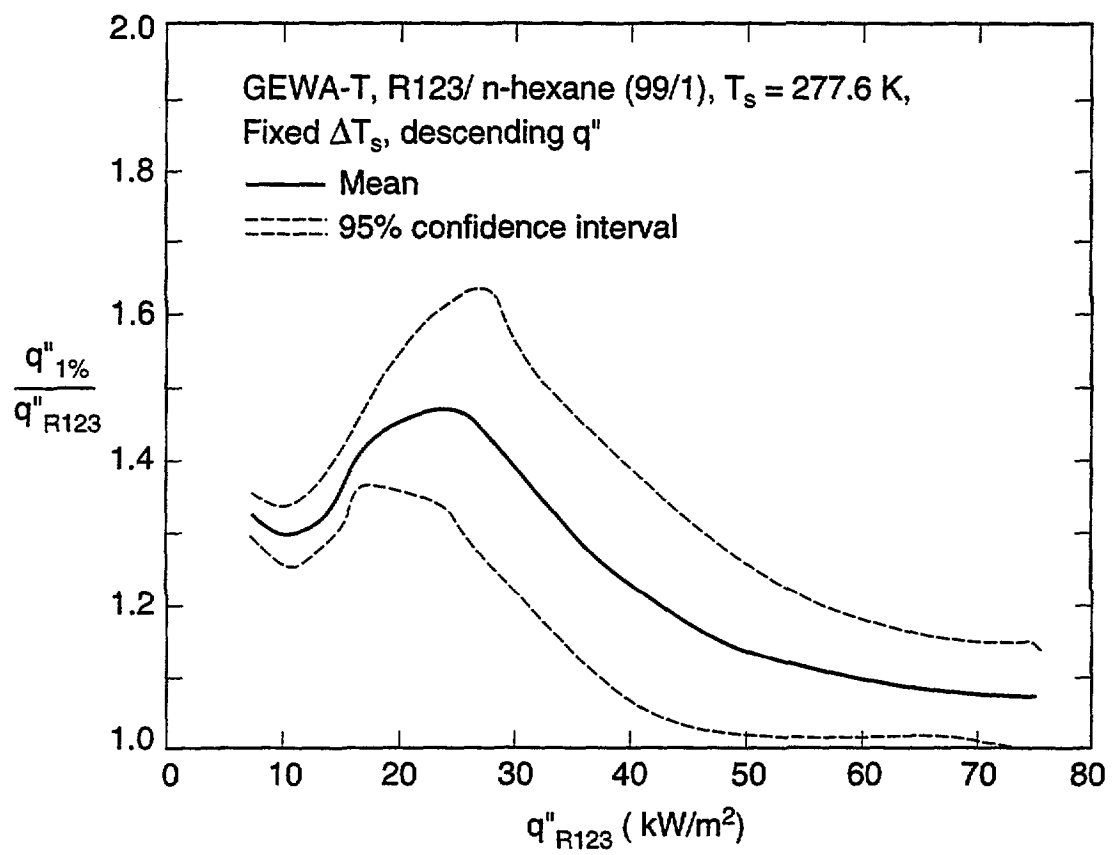


Fig. 10 Enhancement ratio for R123/hexane (99/1) with 95% simultaneous confidence intervals

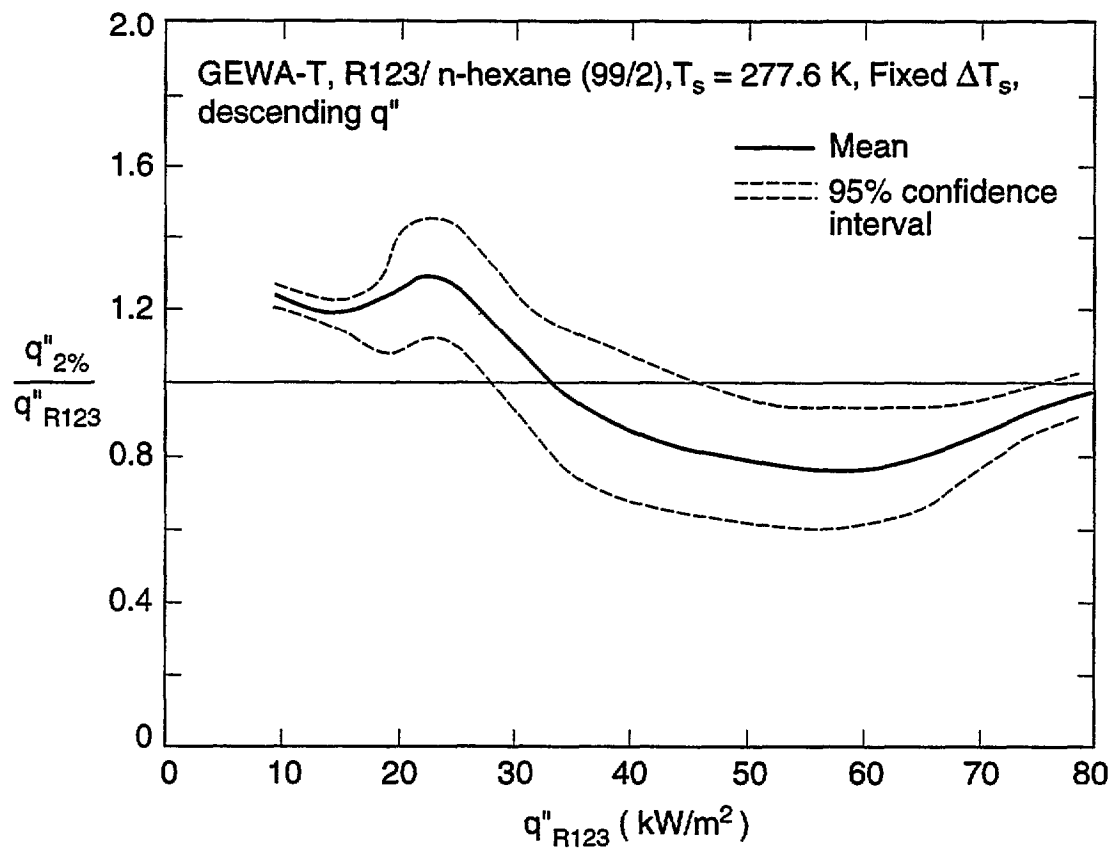
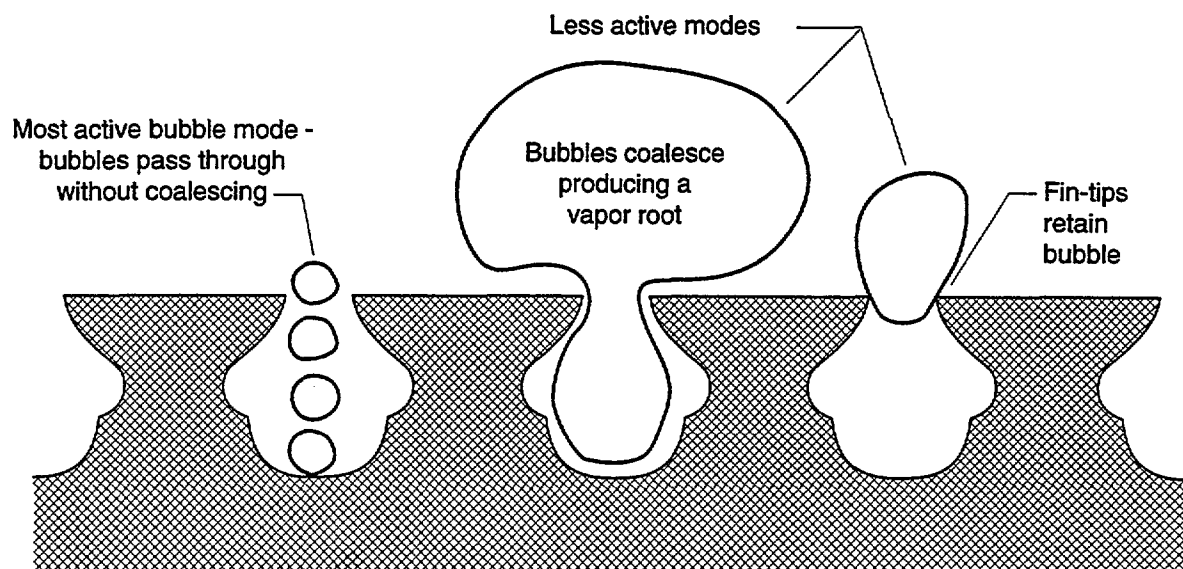


Fig. 11 Enhancement ratio for R123/hexane (98/2) with 95% simultaneous confidence intervals



Three different modes of bubble evolution

Fig. 12 Three boiling modes for R123 at 70 kW/m<sup>2</sup>

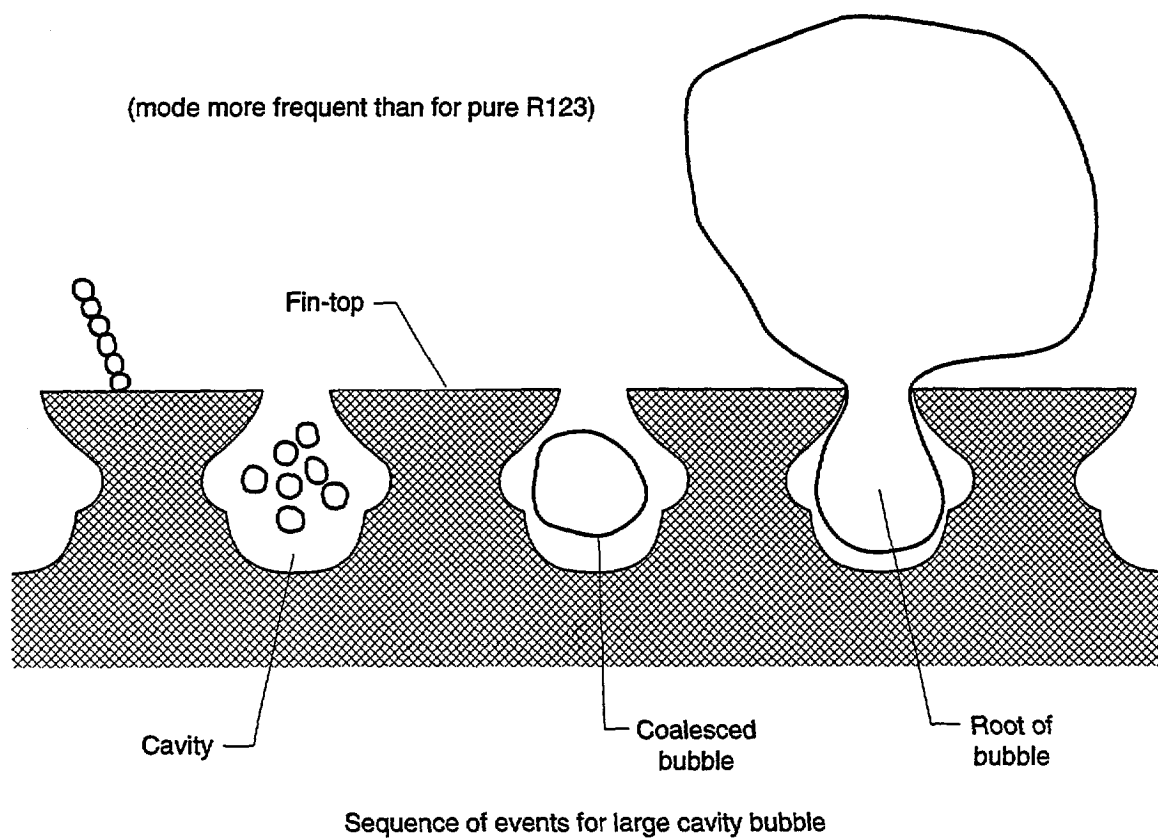


Fig. 13 Bubble activity for R123/hexane (99/1) at  $70 \text{ kW/m}^2$

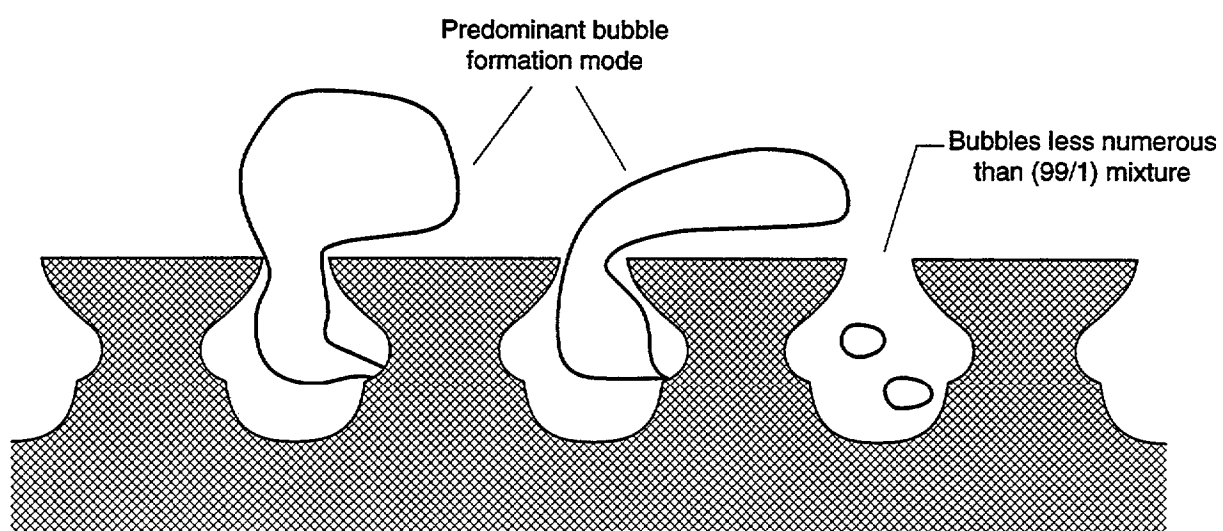


Fig. 14 Bubble activity for R123/hexane (98/2) at 70 kW/m<sup>2</sup>



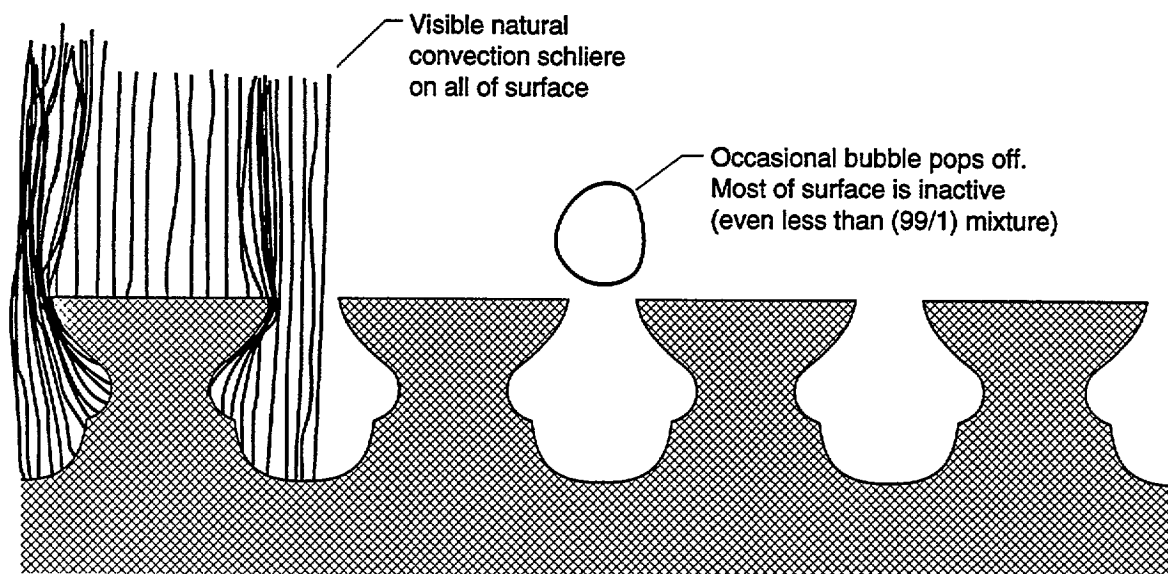
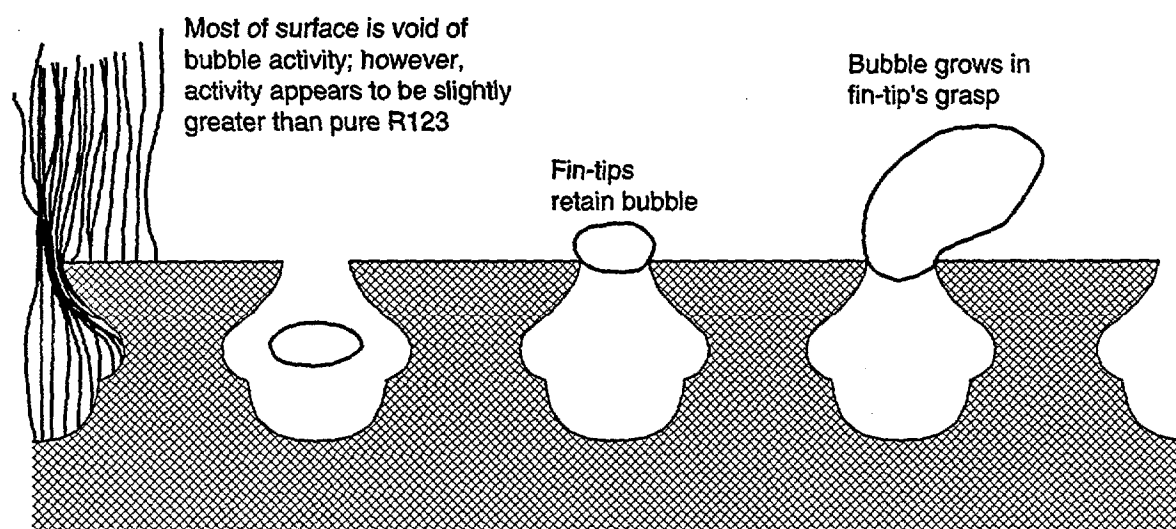


Fig. 15 Bubble activity for R123 at  $30 \text{ kW/m}^2$



Sequence of events for intermediate size cavity bubble

Fig. 16 Bubble activity for R123/hexane (99/1) at  $30 \text{ kW/m}^2$

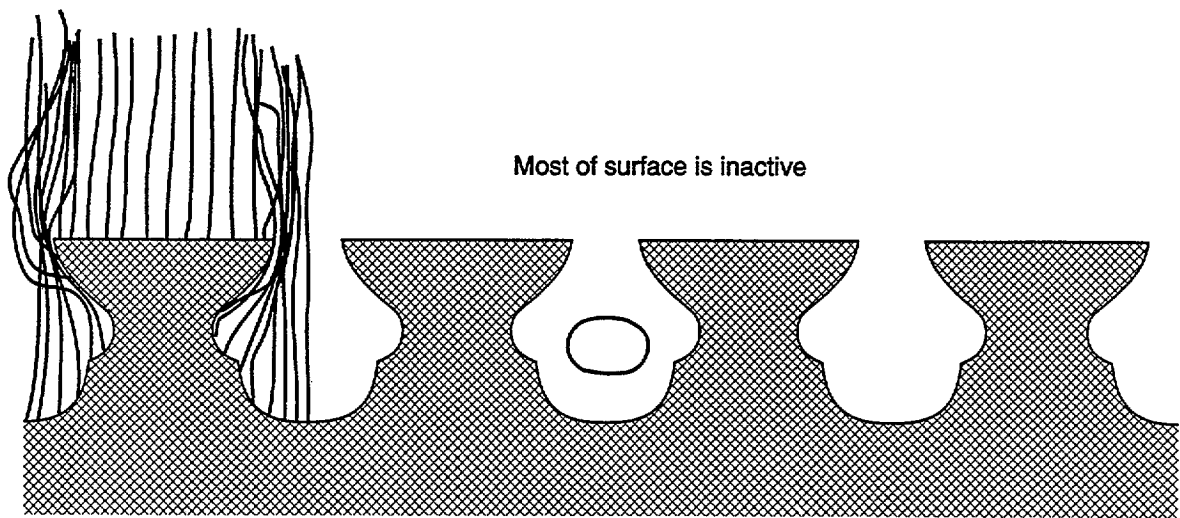


Fig. 17 Bubble activity for R123/hexane (99/2) at  $30 \text{ kW/m}^2$

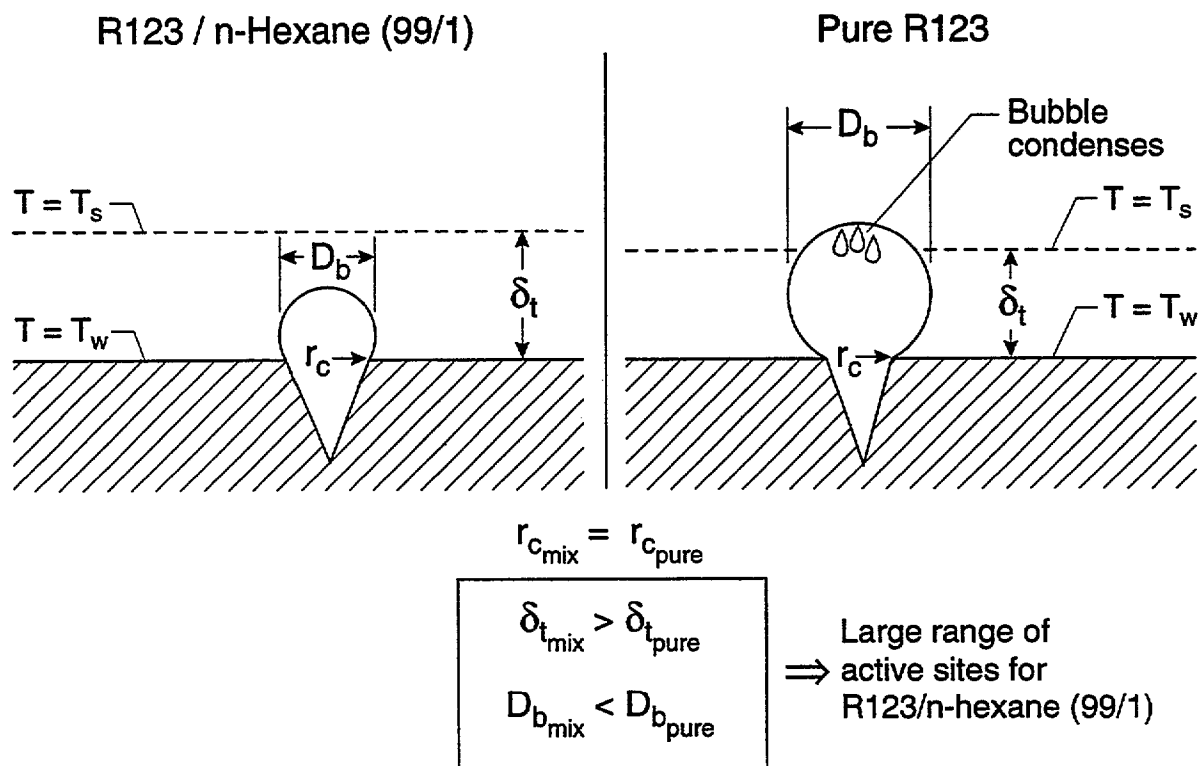


Fig. 18                      Site density enhancement model